6228–6237 *Nucleic Acids Research, 2017, Vol. 45, No. 10* *Published online 10 April 2017*
doi: 10.1093/nar/gkx252

Structural basis for the *D*-stereoselectivity of human DNA polymerase β

Rajan Vyas[1,†], Andrew J. Reed[1,2,†], Austin T. Raper[1,2], Walter J. Zahurancik[1,2], Petra C. Wallenmeyer[1] and Zucai Suo[1,2,*]

[1]Department of Chemistry and Biochemistry, The Ohio State University, Columbus, OH 43210, USA and [2]The Ohio State Biochemistry Program, The Ohio State University, Columbus, OH 43210, USA

Received December 16, 2016; Revised March 24, 2017; Editorial Decision March 27, 2017; Accepted April 03, 2017

ABSTRACT

Nucleoside reverse transcriptase inhibitors (NRTIs) with *L*-stereochemistry have long been an effective treatment for viral infections because of the strong *D*-stereoselectivity exhibited by human DNA polymerases relative to viral reverse transcriptases. The *D*-stereoselectivity of DNA polymerases has only recently been explored structurally and all three DNA polymerases studied to date have demonstrated unique stereochemical selection mechanisms. Here, we have solved structures of human DNA polymerase β (hPolβ), in complex with single-nucleotide gapped DNA and *L*-nucleotides and performed pre-steady-state kinetic analysis to determine the *D*-stereoselectivity mechanism of hPolβ. Beyond a similar 180° rotation of the *L*-nucleotide ribose ring seen in other studies, the pre-catalytic ternary crystal structures of hPolβ, DNA and *L*-dCTP or the triphosphate forms of antiviral drugs lamivudine ((-)3TC-TP) and emtricitabine ((-)FTC-TP) provide little structural evidence to suggest that hPolβ follows the previously characterized mechanisms of *D*-stereoselectivity. Instead, hPolβ discriminates against *L*-stereochemistry through accumulation of several active site rearrangements that lead to a decreased nucleotide binding affinity and incorporation rate. The two NRTIs escape some of the active site selection through the base and sugar modifications but are selected against through the inability of hPolβ to complete thumb domain closure.

INTRODUCTION

Replication fidelity is partially determined by the preference of DNA polymerases (Pols) to form correct G:C and A:T Watson–Crick base pairs. Many factors including hydrogen bonding with the incoming nucleotide (1,2), minor groove interactions with active site residues (3,4) and base stacking (5), affect fidelity to varying degrees among different DNA Pols. The structural basis for the inherent *D*-stereoselectivity of DNA Pols is not as well-defined despite wide-spread use of numerous clinically successful antiviral nucleotide analog reverse transcriptase inhibitors (NRTIs) possessing non-natural *L*-stereochemistry. Two of the NRTIs approved to treat HIV infection are the *L*-deoxycytidine analogs, lamivudine ((-)3TC; (-)-β-*L*-2′,3′-dideoxy-3′-thiacytidine) and its 5-fluorinated derivative, emtricitabine ((-)FTC; (-)-β-*L*-2′,3′-dideoxy-5-fluoro-3′-thiacytidine), which are activated by host kinases to their respective triphosphate forms, (-)3TC-TP and (-)FTC-TP (Figure 1). Upon nucleotide incorporation catalyzed by viral reverse transcriptases (RTs), viral DNA synthesis is terminated due to the absence of a 3′-OH on the deoxyribose moiety of the NRTIs. Interestingly, both lamivudine and emtricitabine have been shown to be more effective at inhibiting HIV-1 RT and less toxic than their *D*-enantiomers (6–10).

Despite the high clinical efficacy of NRTIs, there are often various drug toxicities associated with usage of these analogs. This is not surprising considering DNA Pols and RTs share a common mechanism for nucleotide incorporation and therefore, likely share a similar mechanism of nucleotide selection (11). For example, NRTI-induced genomic instability and mitochondrial toxicity have been associated with inhibition of human B-family DNA Pols (α, δ and ϵ) (12–14) and human A-family DNA Pol γ (hPolγ) (15,16), respectively. Furthermore, it is likely that DNA Pols possessing lower fidelity such as those involved in DNA damage repair and lesion bypass are able to incorporate the NRTIs more easily and disrupt DNA replication and therefore, may account for the observed *in vivo* drug toxicities. Consistently, our recent kinetic investigations of NRTI incorporation by human DNA Pols from the X- (DNA dam-

*To whom correspondence should be addressed. Tel: +1 614 688 3706; Fax: +1 614 292 6773; Email: suo.3@osu.edu
†These authors contributed equally to the paper as first authors.
Disclaimer: Any opinions, findings, and conclusions expressed in this material are those of the author(s) and do not necessarily reflect those of the Pelotonia Fellowship Program.

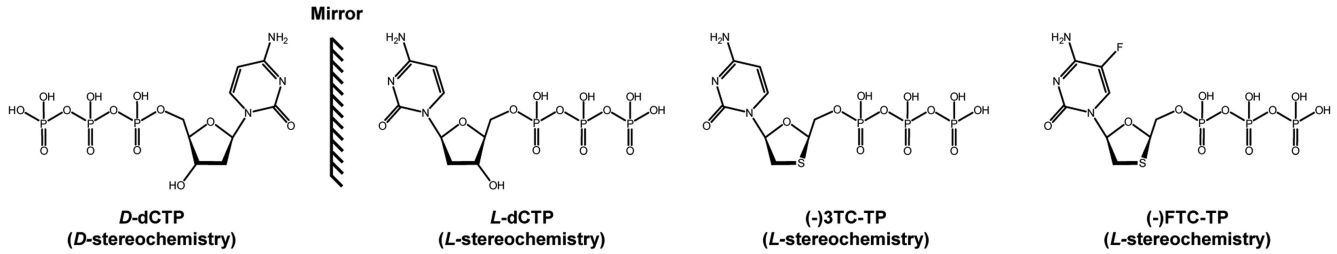

Figure 1. Chemical structures of *D*-dCTP, *L*-dCTP, (-)3TC-TP and (-)FTC-TP. *D*-dCTP and *L*-dCTP are the enantiomers of dCTP. (-)3TC-TP and (-)FTC-TP are the biologically active triphosphate forms of lamivudine [(-)3TC; (-)-β-*L*-2′,3′-dideoxy-3′-thiacytidine] and emtricitabine [(-)FTC; (-)-β-*L*-2′,3′-dideoxy-5-fluoro-3′-thiacytidine], respectively, and analogs of *L*-dCTP.

age repair; hPolβ and λ) (17) and Y-families (DNA lesion bypass; human Pols η, ι, κ and Rev1) (18) demonstrate that these Pols are more susceptible to inhibition by NRTIs than replicative Pols and in some instances incorporate the NRTIs as efficiently as HIV-1 RT. The increased inhibition and efficiency of NRTI incorporation by the X- and Y-family Pols are likely attributed to the lack of 3′→5′ proofreading capability as well as a more flexible active site in each of these damage repair or lesion bypass Pols (17,18).

Although NRTIs with *L*-stereochemistry possess known drug toxicities associated with the ability of host Pols to incorporate such drugs, only recently has a structural basis for the mechanism of *L*-nucleotide incorporation been investigated. Our recent publications detailing the mechanism of *D*-stereoselectivity for hPolλ (19) and *Sulfolobus solfataricus* DNA polymerase IV (Dpo4) (20), model X- and Y-family Pols, respectively, are the first structures to demonstrate the binding and incorporation of *L*-nucleotides and NRTIs with *L*-stereochemistry. Interestingly, hPolλ and Dpo4 utilize different mechanisms to achieve their strong *D*-stereoselectivity of 1.2×10^4 (19) and 4.4×10^4 (20), respectively. Dpo4 selects against *L*-stereochemistry by driving an *L*-nucleotide to adopt non-productive triphosphate binding conformations which have moderately longer distances (2.0–4.4 Å) between the α-phosphate of the *L*-nucleotide and the reacting primer 3′-OH than the distance with a natural *D*-dNTP (20). In comparison, hPolλ initially binds an *L*-nucleotide in a non-productive mode via unique hydrogen bonds between the side chain of R517 and the *L*-dNTP, thereby forcing the reacting 3′-OH of the primer and the α-phosphate of the nucleotide to be much farther apart (9.1–9.3 Å) (19). This non-productive binding mode isomerizes into a productive mode prior to catalysis (19).

It is unclear if the observed differences in *D*-stereoselectivity between Dpo4 and hPolλ arise due to the evolutionary differences between the Pol families. To examine if Pols from the same family exhibit a conserved mechanism of *D*-stereoselectivity, we have co-crystallized and solved the structures of hPolβ (Supplementary Figure S1), an X-family Pol with high sequence homology to hPolλ, in complex with a single-nucleotide gapped DNA substrate and either *L*-dCTP, (-)3TC-TP or (-)FTC-TP (Figure 1) bound at the active site. Furthermore, we measured the incorporation rates and binding affinities of wild-type hPolβ for the various *L*-nucleotides to directly compare with published kinetic studies of hPolλ (19) and Dpo4 (20). In addition, we performed similar kinetic assays with an hPolβ R283 to alanine mutant (R283A) to determine if R283 in hPolβ exhibits a similar role in nucleotide selection to the analogous R517 residue in hPolλ. Collectively, these structural and kinetic studies reveal a mechanism of *D*-stereoselectivity for hPolβ that is distinct from either of those described for hPolλ or Dpo4.

MATERIALS AND METHODS

Preparation of protein and DNA

Human full-length hPolβ was overexpressed and purified as described previously (21). DNA oligomers were purchased from Integrated DNA Technologies and were purified by denaturing polyacrylamide gel electrophoresis. Crystallization oligomers consisted of a 16-mer template (5′-CCGACGGCGCATCAGC-3′), a 10-mer upstream primer (5′-GCTGATGCGC-3′) and a 5-mer downstream 5′-phosphorylated primer (5′-pGTCGG-3′) as described previously (22). Template, upstream primer and downstream primer crystallization oligos were mixed in a 1:1:1 ratio and annealed by heating to 95°C for 5 min followed by slowly cooling to 4°C to form a 1 mM DNA substrate. The 21-19A-41GT-mer DNA substrate reported earlier was used for kinetic studies and consisted of a 41-mer template, a 21-mer upstream primer and a 19-mer downstream 5′-phosphorylated primer (17). To visualize product formation the 21-mer primer of the 21-19A-41GT-mer was radiolabeled with [γ-^{32}P]ATP and OptiKinase according to the manufacturer's protocol, and the unreacted [γ-^{32}P]ATP was subsequently removed via a Bio-Spin 6 column. The DNA substrate was annealed at a 1:1.25:1.15 ratio of upstream primer to downstream primer to template. The *L*-nucleotides, *L*-dCTP, (-)FTC-TP and (-)3TC-TP were obtained from Jena Bioscience.

Pre-steady-state kinetic assays

All fast reactions were performed by using a rapid chemical quench-flow apparatus (KinTek), as previously described (17). Briefly, a pre-incubated solution of full-length wild-type hPolβ or its R283A mutant (300 nM) and 30 nM [^{32}P]-labeled-21-19A-41GT-mer was mixed with varying concentrations of a nucleotide in buffer L (50 mM Tris-HCl, pH 8.4, 5 mM $MgCl_2$, 100 mM NaCl, 0.1 mM ethylenediaminetetraacetic acid (EDTA), 5 mM dithiothreitol (DTT),

Table 1. Pre-steady-state kinetic parameters for single nucleotide incorporation

Nucleotide	k_p (s^{-1})	K_d (μM)	k_p/K_d ($\mu M^{-1}s^{-1}$)	*D*-Stereoselectivity[†]	$R_{D\text{-stereoselectivity}}$[$]
Catalyzed by wild-type hPolβ					
D-dCTP*	5.02 ± 0.07	0.71 ± 0.04	7.1		
L-dCTP	0.00059 ± 0.00002	22 ± 2	2.7×10^{-5}	2.6×10^5	
(-)3TC-TP*	0.0039 ± 0.0001	0.18 ± 0.02	2.2×10^{-2}	323	
(-)FTC-TP*	0.027 ± 0.001	11 ± 2	2.5×10^{-3}	2.9×10^3	
Catalyzed by the R283A mutant of hPolβ					
D-dCTP	0.39 ± 0.02	41 ± 6	9.5×10^{-3}		
L-dCTP	0.00036 ± 0.00006	1110 ± 370	3.2×10^{-7}	3.0×10^4	8.7
(-)3TC-TP	0.0068 ± 0.0003	17 ± 2	4.0×10^{-4}	24	13
(-)FTC-TP	0.0063 ± 0.0002	24 ± 3	2.6×10^{-4}	37	78

An incoming nucleotide was incorporation opposite dG in the single-nucleotide gapped DNA substrate 21-19A-41GT-mer catalyzed by wild-type hPolβ and the R283A mutant of hPolβ at 37°C.
*Reference 17.
[†] *D*-stereoselectivity = $(k_p/K_d)_{D\text{-dCTP}}/(k_p/K_d)_{L\text{-nucleotide}}$.
[$] $R_{D\text{-stereoselectivity}}$ is defined as the ratio: (*D*-stereoselectivity of wild-type hPolβ)/(*D*-stereoselectivity of the R283A mutant of hPolβ).

10% glycerol and 0.1 mg/ml bovine serum albumin) at 37°C. After various times, the reaction was stopped with 0.37 M EDTA and analyzed by sequencing gel electrophoresis. Each time course of product formation was fit to a single-exponential equation, [product] = A[1 - exp(- k_{obs}t)], using KaleidaGraph (Synergy Software) to yield a reaction amplitude (A) and an observed rate constant of nucleotide incorporation (k_{obs}). The k_{obs} values were then plotted against nucleotide concentrations and the data were fit to a hyperbolic equation, $k_{obs} = k_p$[dNTP]/([dNTP] + K_d), to yield an apparent equilibrium dissociation constant (K_d) and a maximum nucleotide incorporation rate constant (k_p).

hPolβ crystallization and structure determination

Purified hPolβ was dialyzed into a buffer containing 50 mM sodium acetate (pH 5.5), 75 mM NaCl, 5% glycerol and 0.1 mM DTT and concentrated to 20 mg/ml as described previously (23). Binary complexes were prepared by mixing purified hPolβ and DNA (1 mM) in a 1:1 ratio at 4°C followed by heating to 35°C and subsequent cooling to room temperature (24). Binary crystals were obtained by hanging drop vapor diffusion against a reservoir solution containing 50 mM imidazole, pH 7.5, 16–18% PEG3350 and 350 mM sodium acetate (24). Binary crystals were then seeded into freshly prepared ternary complex solution (hPolβ:DNA, 10 mM $CaCl_2$ and 2 mM *L*-dNTP) to obtain pre-catalytic ternary crystals at room temperature as described previously (25). The resulting pre-catalytic ternary crystals were harvested and transferred briefly to a cryosolution containing 15% ethylene glycol, 50 mM imidazole (pH 7.5), 20% PEG3350, 90 mM sodium acetate before they were flash frozen in liquid nitrogen. X-ray diffraction data were collected using the LRL-CAT beamline facilities at Advance Photon Source, Argonne National Laboratory. X-ray diffraction data were processed using MOSFLM (26) and structures were solved using the molecular replacement method by PHASER (27) using a previous structure (PDB code: 4KLD) (22) in the absence of ligands and solvent molecules as the initial model. Structural refinement was carried out using REFMAC5 (28). COOT (29) was used for visualization and model building. Quality of the models was assessed using PROCHECK (30). Figures were created using PYMOL (31).

RESULTS

Pre-steady-state kinetics of wild-type hPolβ-catalyzed *L*-nucleotide incorporation

To determine how efficiently *L*-nucleotides are bound and incorporated by hPolβ, we performed single-nucleotide incorporation assays to measure a maximum incorporation rate constant (k_p) and an apparent equilibrium dissociation constant (K_d) for *L*-dCTP (Table 1 and Supplementary Figure S2). This pre-steady state kinetic analysis of hPolβ with *L*-dCTP complements our previous work with hPolβ (17) incorporating (-)3TC-TP and (-)FTC-TP and confirms that each *L*-nucleotide is incorporated slower and with an efficiency (k_p/K_d) two to five orders of magnitude lower than the k_p/K_d value for *D*-dCTP (Table 1). Unlike hPolλ, which displays a similarly tight nucleotide binding affinity ($1/K_d$) for *L*-dCTP relative to *D*-dCTP (19), the *L*-stereochemistry resulted in a 30-fold decrease in nucleotide binding affinity of hPolβ for *L*-dCTP compared to *D*-dCTP (Table 1 and Supplementary Figure S2). Surprisingly, the chemical modifications (Figure 1) in the sugar rings of (-)3TC-TP and (-)FTC-TP result in significantly different effects on nucleotide binding affinity. While (-)3TC-TP was bound ∼4-fold tighter than *D*-dCTP, the additional fluorination of the base resulted in a 15-fold decrease in nucleotide binding affinity compared to *D*-dCTP (Table 1). Furthermore, hPolβ preferentially incorporated *D*-dCTP over *L*-dCTP with a *D*-stereoselectivity, defined as $(k_p/K_d)_{D\text{-dCTP}}/(k_p/K_d)_{L\text{-dCTP}}$, of 2.7×10^5, while the *D*-stereoselectivity was reduced to only 325 and 2900 for the incorporation of (-)3TC-TP and (-)FTC-TP, respectively (Table 1). Thus, the chemical changes in the ribose of (-)3TC-TP and (-)FTC-TP relaxed the *D*-stereoselectivity of hPolβ by 830- and 100-fold, respectively, making these *L*-nucleotide analogs significantly better substrates than *L*-dCTP.

Pre-steady-state kinetics of the mutant R283A of hPolβ-catalyzed *L*-nucleotide incorporation

To determine if R283 in hPolβ, analogous to R517 in hPolλ, is critical for incorporation of *L*-nucleotides, we generated the R283A substitution mutant and performed single-nucleotide incorporation assays to investigate the effect of this mutation on the kinetic parameters for incorporation of *D*-dCTP, *L*-dCTP, (-)3TC-TP and (-)FTC-TP (Table 1 and Supplementary Figure S3). The mutation resulted in a 13-fold drop in incorporation rate for *D*-dCTP relative to wild-type but only resulted in a small change (0.5- to 4-fold) for the *L*-nucleotides (Table 1 and Supplementary Figure S3). Similarly, the R283A mutation resulted in a large 59-fold decrease in nucleotide binding affinity for *D*-dCTP relative to wild-type (Table 1). In addition, the binding of the *L*-nucleotides was affected to varying degrees with *L*-dCTP, (-)3TC-TP and (-)FTC-TP exhibiting 50-, 94- and 2-fold decreases in binding affinity, respectively. These changes resulted in respective decreases in nucleotide incorporation efficiency (k_p/K_d) of 747-, 84-, 55- and 9.6-fold for *D*-dCTP, *L*-dCTP, (-)3TC-TP and (-)FTC-TP (Table 1). As a result, the *D*-stereoselectivity was relaxed relative to wild-type by 8.7-, 13- and 78-fold for *L*-dCTP, (-)3TC-TP and (-)FTC-TP, respectively (Table 1). Although the *D*-stereoselectivity of the R283A mutant of hPolβ is relaxed, the role of R283 in anchoring the thumb domain (Supplementary Figures S1 and 4) in the closed conformation upon nucleotide binding via a hydrogen bond with the templating base most likely leads to an overall loss in nucleotide selection upon mutation and thus all nucleotides are bound weakly regardless of their *D*- or *L*-stereochemistry.

Structure of hPolβ with bound DNA and *L*-dCTP

To capture a pre-catalytic ternary complex of hPolβ, DNA and *L*-dCTP (hPolβ•DNA•*L*-dCTP), crystallization was performed in the presence of the non-catalytic metal ion, Ca^{2+} (Figure 2A). The pre-catalytic ternary structure of hPolβ•DNA•*L*-dCTP was refined to 1.8 Å (Supplementary Table S1), and the active site shows well-defined electron density for the incoming *L*-dCTP (Figure 2A and Supplementary Figure S5). Similar to the canonical pre-catalytic ternary structure with *D*-dCTP (hPolβ•DNA•*D*-dCTP) (Figure 3A), the base of *L*-dCTP was present in the *anti*-conformation and formed three hydrogen bonds (2.7–3.0 Å) with the templating nucleotide dG (Figures 2A and 3B). Consistent with our earlier structural studies of hPolλ with *L*-nucleotides (19), the constraint imposed by the *L*-stereochemistry combined with Watson–Crick base pairing caused the sugar ring of *L*-dCTP to rotate 180° relative to *D*-dCTP. Beyond the active site differences, the overall quaternary structure of hPolβ•DNA•*L*-dCTP is very similar to the hPolβ•DNA•*D*-dCTP structure (Figure 4A) with an RMSD of 0.76 Å (Supplementary Table S2). Furthermore, in the hPolβ•DNA•*L*-dCTP structure, the dG:*L*-dCTP base pair is sandwiched between the terminal template-primer junction base pair and Helix N of the thumb domain (Figure 2A), as is typical for closed conformation structures with a correct incoming nucleotide (Figures 3A and 4) (22).

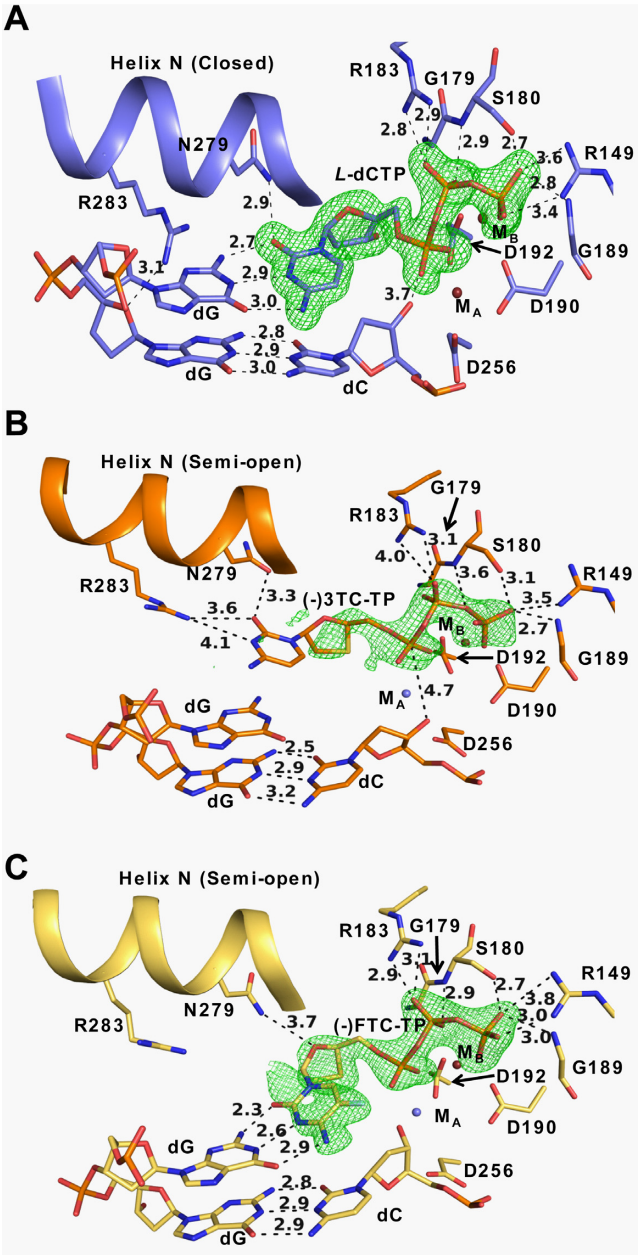

Figure 2. Binding of *L*-nucleotides in the presence of Ca^{2+} within the active site of hPolβ. (**A**) hPolβ•DNA•*L*-dCTP; (**B**) hPolβ•DNA•(-)3TC-TP; and (**C**) hPolβ•DNA•(-)FTC-TP. The F_o-F_c omit maps (3σ level) for the incoming *L*-nucleotides are illustrated in green. The two template nucleotides, the primer 3′-terminal nucleotide and active site residues are displayed as sticks. Hydrogen bonds and the distance between the primer 3′-OH group and the α-phosphorus atom of an incoming *L*-nucleotide are displayed as black dashed lines with the numbers representing the distance in Å. The Ca^{2+} and Na^{+} ions are shown as red and light blue spheres, respectively.

The triphosphate moiety of *L*-dCTP was observed in the productive chair-like conformation, similar to the *D*-dCTP structure (22) and shows similar interactions with the active site divalent metal ions (Figures 2A, 3A, B and 4E). Furthermore, *L*-dCTP exhibits several key active site interactions reminiscent of *D*-dCTP. For example, the side chain

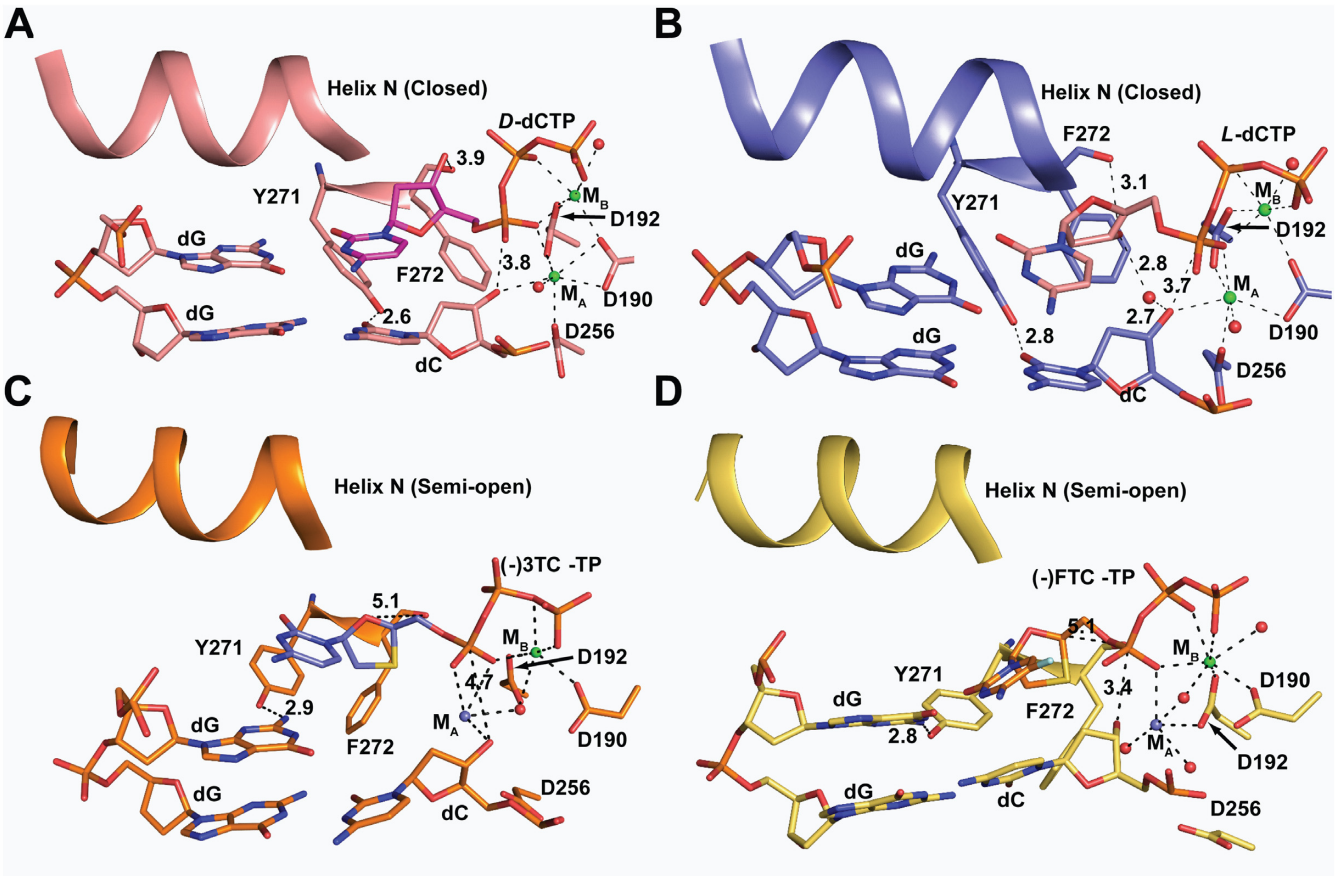

Figure 3. Metal coordination in pre-catalytic ternary structures of hPolβ. (**A**) hPolβ•DNA•*D*-dCTP (4KLD); (**B**) hPolβ•DNA•*L*-dCTP; (**C**) hPolβ•DNA•(-)3TC-TP; and (**D**) hPolβ•DNA•(-)FTC-TP. Hydrogen bonds between coordinating ligands to the metal ions and the distance between the primer 3'-OH group and the α-phosphate atom of the incoming nucleotide are displayed as black dashed lines with the numbers indicating the distance in Å. Water molecules (red), Ca^{2+} ions (green) and Na^{+} ions (light blue), are shown as spheres.

of R283 from Helix-N forms a hydrogen bond with the template strand, the side chain of N279 hydrogen bonds with the incoming nucleotide and the side chain of Y271 forms a hydrogen bond with the base of the primer 3′-terminal nucleotide (Figures 2A, 3A, B and Supplementary Figure S4). The only notable structural differences are the side chain rotation of residue F272, the shortening of the hydrogen bond between the backbone carbonyl of F272 and the 3′-OH of *L*-dCTP, the slight repositioning of the divalent metal ions within the active site and a water molecule that bridges the 3′-OH of *L*-dCTP and the 3'-OH of the primer terminal nucleotide (Figure 3B and Supplementary Figure S6A). These interactions are a direct result of the ribose rotation which causes the 3′-OH of *L*-dCTP and the 3'-OH of the primer terminal nucleotide to point toward each other at a distance of 3.9 Å. Surprisingly, the distance between the primer 3′-OH and the α-phosphate of the incoming nucleotide (3.7 Å) is maintained at a distance similar to the canonical structure of hPolβ•DNA•*D*-dCTP (3.8 Å) despite a potential steric clash between the 3′-OH of *L*-dCTP and the primer 3'-OH (Supplementary Figure S6A and B).

Structures of hPolβ with bound NRTIs

The pre-catalytic ternary complexes of hPolβ, DNA and the NRTIs, (-)3TC-TP (hPolβ•DNA•(-)3TC-TP) and (-)FTC-TP (hPolβ•DNA•(-)FTC-TP), were crystallized in the presence of non-catalytic Ca^{2+}, as was done for the hPolβ•DNA•*L*-dCTP complex. The structures of hPolβ•DNA•(-)3TC-TP and hPolβ•DNA•(-)FTC-TP were refined to 2.2 and 1.8 Å, respectively (Supplementary Table S1). Within the active site of the hPolβ•DNA•(-)3TC-TP structure, the electron density difference map (F_o-F_c) for the triphosphate moiety is well-defined but is less evident for the ribose ring and base portion of the nucleotide (Figure 2B), while in the active site of the hPolβ•DNA•(-)FTC-TP structure, the electron density difference map (F_o-F_c) for the entire nucleotide is well-defined (Figure 2C). However, both *L*-nucleotides agree well with the $2F_o$-F_c electron density map (Supplementary Figure S5B and C). Surprisingly, both *L*-nucleotide analogs exhibited triphosphate moieties in a productive chair-like conformation similar to the *D*-dCTP (22) and *L*-dCTP structures (Figure 4 and Supplementary Figure S1). However, in both structures the thumb domain displays moderate electron density with Helix-N observed in a semi-open conformation (Figure 4) that is intermediate

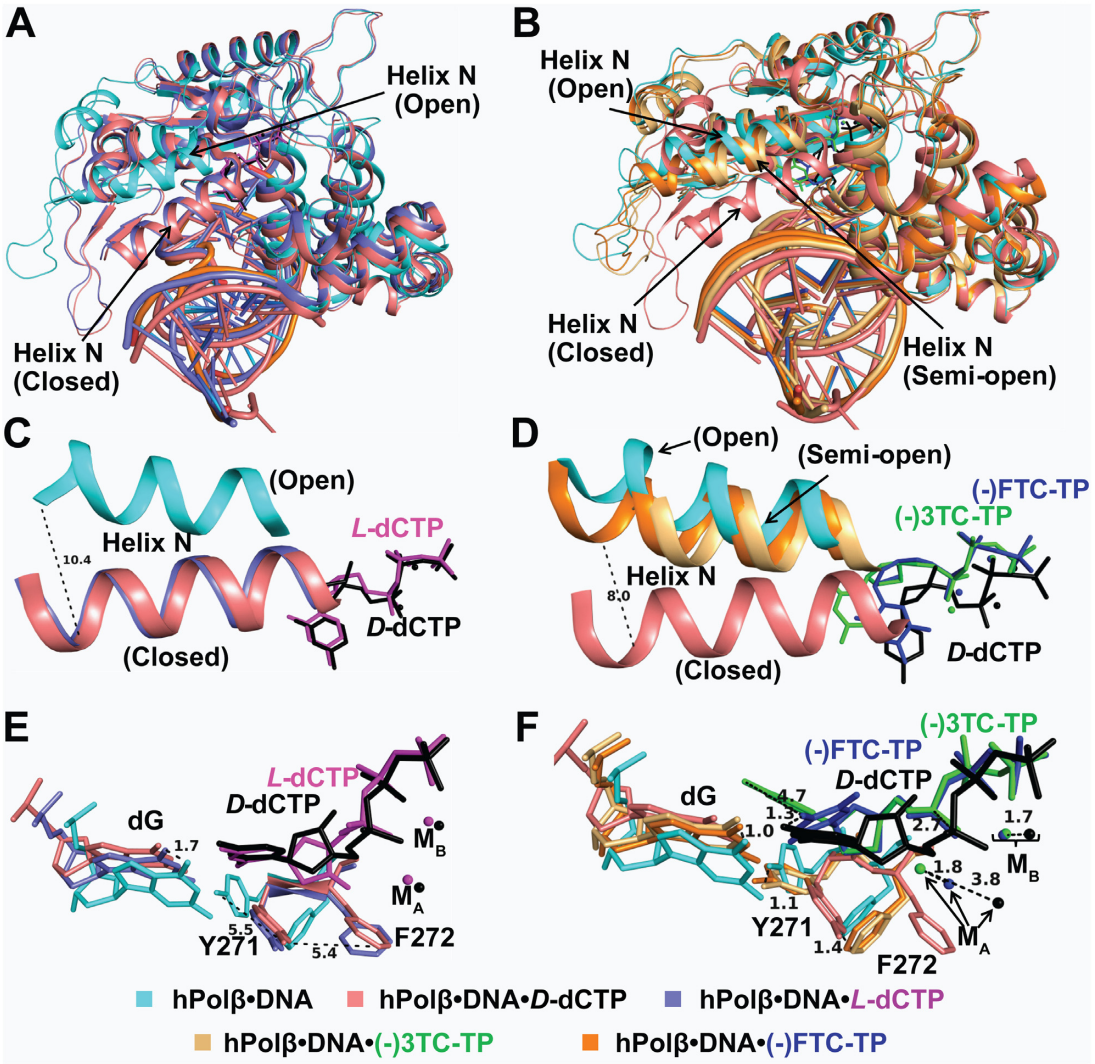

Figure 4. Structural differences between the binary and ternary structures complexed with either a *D*- or an *L*-nucleotide in the presence of Ca^{2+}. (**A**) Superposition of hPolβ•DNA (1BPX), hPolβ•DNA•*D*-dCTP (4KLD) and hPolβ•DNA•*L*-dCTP structures. (**B**) Superposition of hPolβ•DNA (1BPX), hPolβ•DNA•*D*-dCTP (4KLD), hPolβ•DNA•(-)3TC-TP and hPolβ•DNA•(-)FTC-TP structures. (**C** and **D**) Zoomed views of Helix-N conformation adopted in (A) and (B), respectively. (**E** and **F**) Active site differences of structures superimposed in (A) and (B). In (E) and (F) only the templating nucleotide, incoming nucleotide, Y271, F272 and the A-site (M_A) and B-site (M_B) metal ions are presented. In (E) both metal sites are occupied by Ca^{2+} ions. In (F) the M_B site is occupied by Ca^{2+} for all three structures, while the M_A site is occupied by Na^+ ions for the (-)3TC-TP and (-)FTC-TP structures but is a Ca^{2+} ion in the *D*-dCTP structure.

to the open and closed conformations observed in the binary (25) and ternary (22) complex structures, respectively (Supplementary Figure S4).

Although many interactions with the incoming nucleotide and triphosphate are maintained in the hPolβ•DNA•(-)3TC-TP and hPolβ•DNA•(-)FTC-TP structures when compared to the *D*-dCTP (Supplementary Table S2, RMSD of 1.75 and 1.95 Å, respectively) and *L*-dCTP structures, the hydrogen bond between R283 and the templating nucleotide is absent and the side chain of Y271 forms a hydrogen bond with the template nucleotide, rather than the primer 3′-terminal nucleotide (Figure 3). In addition to these structural changes, (-)FTC-TP forms a non-planar Watson–Crick base pair with the templating dG while (-)3TC-TP does not form a Watson–Crick base pair with any nucleotide. Rather (-)3TC-TP is facing the side chain of R283 at a distance too far to form a hydrogen bond (3.6 Å) but maintains a hydrogen bond with N279 (Figure 2B).

Unlike the global conformation of the thumb domain (Supplementary Figure S2), which is intermediate to its position in the binary and the ternary structures, the active sites of the (-)3TC-TP and (-)FTC-TP structures exhibit side chain positions that resemble either the binary or ternary structures. For example, the side chain positions of F272 and D190 are similar to the binary complex while those of D192 and R258 resemble the ternary complex. This mixed active site structure, consisting of both binary and ternary features, disrupts metal ion coordination and causes the primer 3′-OH, the A-site metal ion and α-phosphate to significantly move (2.4–3.9 Å) relative to the *D*-dCTP structure (Figure 4F and Supplementary Figure S6). As a result of

these movements, the coordination number, distances and geometries were altered for the A-site metal ion and were inconsistent with what is expected for a Ca^{2+} ion and therefore was rather modeled as a Na^{+} ion (Figure 4F). Remarkably, the distance from the primer 3′-OH to the α-phosphate of the nucleotide for (-)FTC-TP (3.4 Å) is comparable to the *L*-dCTP (3.7 Å) and *D*-dCTP (3.8 Å) structures despite the movement of the reacting groups and the altered metal ion geometry (Figure 3 and Supplementary Figure S6). However, the distance between reacting groups for the hPolβ•DNA•(-)3TC-TP structure (4.7 Å) is significantly lengthened compared to the other three nucleotides (Figure 4 and Supplementary Figure S6).

DISCUSSION

Comparison to previously characterized *D*-stereoselectivity mechanisms

To date, the *D*-stereoselectivity mechanism of hPolλ (19) and Dpo4 (20) have been determined as well as the mechanism of drug selectivity of hPolγ (32). All three studies have demonstrated that these Pols use unique methods to establish *D*-stereochemical selection. Dpo4 achieves *D*-stereoselectivity by forcing the *L*-nucleotides to adopt several non-productive triphosphate conformations (20). hPolγ selects between (+) and (-)FTC-TP (equivalent to *D*- and *L*-enantiomers) through an altered Watson–Crick geometry, a direct result of the ribose rotation and a steric clash between the modified ribose of (-)FTC-TP and the side chain of Y951 (32). Interestingly, Y951 of hPolγ is also a selection factor against rNTPs and is analogous to the 'steric gate' residue in DNA Pols (33,34).

Previously, we identified that X-family hPolλ uses two pathways to incorporate nucleotides with *L*-stereochemistry (Supplementary Figure S7) (19). Briefly, in Pathway I, the nucleotide is bound in a catalytically incompetent triphosphate conformation (Supplementary Figure S7, chains I and M) and forms an unusual base pair-like hydrogen bond with the side chain of R517. This is followed by transition to a productive conformation (Supplementary Figure S7, chains A and E) where the canonical Watson–Crick base pair is formed and the triphosphate adopts the productive chair-like conformation. Alternatively, in Pathway II the nucleotide is directly bound in the catalytically competent conformation (Supplementary Figure S7, chains A and E). However, the direct binding of an *L*-nucleotide in a productive conformation is much less efficient, as evident by the severely decreased binding and incorporation of the *L*-nucleotides when Pathway I is abolished by mutation of R517 to alanine (Supplementary Figure S7) (19).

Here, all the structures of hPolβ with the *L*-nucleotides have productive triphosphate binding conformations (Figures 2, 3 and Supplementary Figure S7) and the equivalent 'steric gate' tyrosine residue, Y271, does not clash with the ribose of the *L*-nucleotides (Figure 3A and B). Thus, hPolβ does not utilize either of the selection mechanisms observed with Dpo4 (20) or hPolγ (32). It was expected that hPolβ would follow a mechanism of *D*-stereoselectivity similar to that of hPolλ (19) due to the high degree of sequence, structural, and functional similarity between the C-terminal Polβ-like domain of hPolλ and the full-length hPolβ (35). However, (-)FTC-TP and *L*-dCTP, in the pre-catalytic ternary structures of hPolβ presented here, bind with Watson–Crick base pairs and productive triphosphate conformations that are very similar to those of hPolλ in chain A and E of Pathway II (Figures 2 and 3; Supplementary Figures S7 and S8). Interestingly, the hPolβ•DNA•(-)3TC-TP structure in the presence of Ca^{2+} binds a nucleotide in a position reminiscent to that observed in the Chain I/M hPolλ•DNA•(-)3TC-TP structure (Figure 2B and Supplementary Figure S8). Despite the similar (-)3TC-TP binding conformation, the base portion of (-)3TC-TP in the hPolβ structure is too far (3.6–4.1 Å) to form a hydrogen bond with R283 (Figure 2B), the residue analogous to the critical R517 in hPolλ. This increased distance and failure to form stable hydrogen bonds between (-)3TC-TP and R283 suggests that this Pathway I-like binding conformation of *L*-nucleotides may be unfavorable for hPolβ (Figure 2B and Supplementary Figure S8). To test this hypothesis, we performed an analogous pre-steady-state investigation of the R283A mutation (Table 1 and Supplementary Figure S3). We determined that the mutation resulted in a decreased incorporation rate and nucleotide binding affinity for *D*-dCTP and all three *L*-nucleotides (Table 1) and relaxed the *D*-stereoselectivity by 8.7- to 78-fold, relative to wild-type. This is suggestive of an alternative binding mode between the R283A side chain and the *L*-nucleotides similar to that of chain I and M of hPolλ, and that removal of this interaction results in weakened binding affinities and selection for the *L*-nucleotides. However, the R517A mutation in hPolλ resulted in a similar 54-fold decrease in binding affinity for *L*-dCTP compared to wild-type hPolλ, but increased the binding affinity for natural *D*-dCTP by 4-fold (19). Therefore, the loss of incorporation efficiency for both *D*- and *L*-nucleotides for the R283A mutant of hPolβ suggests that R283 in hPolβ has a different role compared to R517 in hPolλ. Thus, it is likely that the weakened binding affinity and *D*-stereoselectivity observed with the R283A hPolβ mutant are coincidental and arise from an inherent inability to stabilize the closed conformation as evident by the similar drop (50- to 94-fold) in binding affinity for *D*-dCTP, *L*-dCTP and (-)3TC-TP (Table 1). In addition, the absence of binding conformations similar to hPolλ chain I and M in the hPolβ•DNA•(-)FTC-TP and hPolβ•DNA•*L*-dCTP structures suggests that hPolβ uses a mechanism distinct from that of hPolλ. Furthermore, as the major factors allowing hPolλ to select against *L*-stereochemistry are due to the differences between Pathways I and II (Supplementary Figure S7), a unique and more efficient selection mechanism against *L*-nucleotides must be employed by hPolβ to account for the observed 22-, 7- and 24-fold higher selectivity against *L*-dCTP, (-)3TC-TP and (-)FTC-TP, respectively, when compared to hPolλ (17).

Structural basis for the *D*-stereoselectivity of hPolβ

Unlike hPolλ (36), nucleotide incorporation by hPolβ requires a large conformational change that results in the N-helix of the thumb domain clasping down on the nascent base pair, effectively securing the reacting groups and op-

timally positioning them for catalysis (37). It is widely thought that such conformational changes or differences in nucleotide-bound complexes may act as fidelity checkpoints during single-nucleotide incorporation to preferentially select correct over incorrect nucleotides. However, the exact mechanism by which the conformational changes or differences in conformations of bound complexes affect Pol fidelity has long been debated (11,25,38–48). Regardless of the mechanism, it is clear that the closure of the thumb domain is important for efficient nucleotide incorporation (49) and therefore, it was expected that the conformation of hPolβ would play a role in selecting against nucleotides with *L*-stereochemistry.

Surprisingly, the hPolβ•DNA•*L*-dCTP structure is observed in the closed conformation and seemingly escapes any conformational selection checkpoints. However, several active site rearrangements occur compared to the hPolβ•DNA•*D*-dCTP structure (Figure 3, Supplementary Figures S1 and S10). Many of the atoms of the incoming *L*-dCTP have been shifted (0.3–1.8 Å, Supplementary Figure S10) compared to the respective atoms in the incoming *D*-dCTP of the hPolβ•DNA•*D*-dCTP structure. In addition, the A- and B-site metal ions shift by 0.79 and 0.73 Å, respectively (Supplementary Figure S10). Moreover, similar to the hPolλ•DNA•*L*-dCTP structure (19), a water molecule is observed bridging the 3′-OH of *L*-dCTP (2.82 Å) and the primer 3′-OH (2.62 Å), which likely weakens the ability of the primer 3′-OH to act as a nucleophile during nucleotide incorporation (Figure 3B and Supplementary Figure S6B). The ribose rotation also positions the 3′-OH of *L*-dCTP near the hydrophobic side chain of F272, which results in the side chain rotating slightly from its position in the hPolβ•DNA•*D*-dCTP structure (Figure 4E) and likely further weakens the binding of *L*-dCTP. Together, these active site alterations establish the *D*-stereoselectivity of hPolβ and result in an overall decreased nucleotide binding affinity and incorporation rate for *L*-dCTP incorporation (24 μM and 0.00063 s^{-1}, respectively, Table 1) compared to the incorporation of natural *D*-dCTP (0.71 μM and 5.02 s^{-1}, respectively, Table 1).

Conformational change in the drug selectivity of hPolβ

While it was unexpected that the large conformational change exhibited by hPolβ would not contribute to the mechanism of *D*-stereoselectivty, the ability of *L*-dCTP to support domain closure can be attributed to a key hydrogen bond between the 3′-OH of *L*-dCTP and the backbone carbonyl of F272 (Figure 3B and Supplementary Figure S6B). This hydrogen bond stabilizes the thumb domain in the closed conformation and is similar to that seen in the hPolβ•DNA•*D*-dCTP structure, where the 3′-OH of *D*-dCTP forms a hydrogen bond with the backbone carbonyl of T273 (22). Notably, nucleotide binding is known to stabilize the rotation of the F272 side chain to its position in the ternary complex (25). This rotation results in the disruption of the salt bridge formed between D192 and R258 in the binary complex and allows the side chain of D192 to rotate and bind the catalytic A-site metal ion during the formation of a productive ternary complex (25).

In contrast, as the NRTIs, (-)3TC-TP and (-)FTC-TP, lack a 3′-OH and cannot form a hydrogen bond with the N-helix and would not stabilize the closed conformation to the same extent as *L*- and *D*-dCTP (Supplementary Figure S6C and D). This is clearly evident by the inability of the thumb domain to fully close in the hPolβ•DNA•(-)3TC-TP and hPolβ•DNA•(-)FTC-TP structures (Figure 4D). Furthermore, the geometrical strain induced by the 180° rotation of the ribose results in non-planar ((-)FTC-TP) or absent ((-)3TC-TP) Watson–Crick base pairing between the NRTIs and the templating nucleotide. Thus, it is likely that a combination of these two aspects prohibit full closure of the thumb domain. Notably, the distance between the α-phosphate of the incoming (-)3TC-TP and the primer 3′-OH (4.7 Å, Figure 3C and Supplementary Figure S6C) is too large for catalysis to occur and accounts for the reduced incorporation rate (0.0039 s^{-1}, Table 1) compared to *D*-dCTP (5.02 s^{-1}, Table 1). On the other hand, despite the inability to close fully, the distance between the α-phosphate of the incoming (-)FTC-TP and the primer 3′-OH (3.4 Å, Figure 3D and Supplementary Figure S6D) is very similar to the distances observed for both *L*-dCTP (3.7 Å, Figure 3B) and *D*-dCTP (3.8 Å, Figure 3A) and likely results in the higher observed incorporation rate (0.027 s^{-1}, Table 1) compared to (-)3TC-TP.

The inability of the NRTIs to support domain closure would seemingly make these nucleotides worse substrates but this is not the case considering the observed increased binding affinities and incorporation rates of (-)3TC-TP (0.18 μM and 0.0039 s^{-1}, respectively, Table 1) and (-)FTC-TP (11 μM and 0.027 s^{-1}, respectively, Table 1) compared to *L*-dCTP (24 μM and 0.00063 ± s^{-1}, respectively, Table 1). The substitution of the C3′ atom of *L*-dCTP with a more electron-rich sulfur in the NRTIs accounts for the increased binding affinity through an enhanced stacking interaction with the active site residues, F272 and Y271 (Supplementary Figure S9). Furthermore, the lack of the steric clash between the NRTI 3′-OH and primer 3′-OH or Y271 may allow optimal alignment of the reacting groups to occur more readily following full domain closure (Supplementary Figure S6). The differences in binding affinities of (-)3TC-TP (0.18 μM, Table 1) and (-)FTC-TP (11 μM, Table 1) are likely associated with the addition of the fluorine group to the cytosine base of (-)FTC-TP. As this fluorine group withdraws electrons from the base, the stacking interaction between the base of (-)FTC-TP and the primer 3′-terminal base may be weakened and may disfavor the binding of (-)FTC-TP to some degree.

Overall, the structures presented here demonstrate that the mechanism of *D*-stereoselectivity by hPolβ consists of the accumulation of several minor active site rearrangements that ultimately disfavor the binding and incorporation of nucleotides that have *L*-stereochemistry rather than through alternative nucleotide and triphosphate binding modes seen with other polymerases (19,20). Interestingly, hPolβ exhibits a protein conformational selection against NRTIs that have a sulfur substituted ribose. However, this substitution allows (-)3TC-TP and (-)FTC-TP to escape some of the active site alterations associated with the presence of the 3′-OH in *L*-dCTP, and therefore these NRTIs are more efficiently incorporated. Without an evident unifying

mechanism for *D*-stereoselectivity, it remains necessary to investigate how replicative DNA polymerases or the target of the NRTIs, HIV RT, select against nucleotides with *L*-stereochemistry. Such an investigation would provide valuable insight into novel drug design and potentially limit the cytotoxicity associated with *L*-nucleotide drugs.

ACCESSION NUMBERS

PDB accession codes: 5U2R (hPolβ•DNA•*L*-dCTP), 5U2S (hPolβ•DNA•(-)3TC-TP) and 5U2T (hPolβ•DNA•(-)FTC-TP).

SUPPLEMENTARY DATA

Supplementary Data are available at NAR Online.

ACKNOWLEDGEMENTS

We would like to thank Dr. Joy Feng of Gilead Sciences, Inc. for supplying the *L*-nucleotides used for crystallization. This research used resources of the Advanced Photon Source, a U.S. Department of Energy (DOE) Office of Science User Facility operated for the DOE Office of Science by Argonne National Laboratory. Use of the Lilly Research Laboratories Collaborative Access Team (LRL-CAT) beamline at Sector 31 of the Advanced Photon Source was provided by Eli Lilly Company, which operates the facility.

FUNDING

National Institutes of Health Grants [ES024585, ES026821 to Z.S.]; National Institutes of Health Training Grant Graduate Fellowship [T32GM008512 to A.T.R.]; Pelotonia Fellowship (to W.J.Z.); U.S. Department of Energy (DOE) Office of Science User Facility [DE-AC02-06CH11357]. Funding for open access charge: NIH Grant [ES024585].
Conflict of interest statement. None declared.

REFERENCES

1. Lee,H.R., Helquist,S.A., Kool,E.T. and Johnson,K.A. (2008) Base pair hydrogen bonds are essential for proofreading selectivity by the human mitochondrial DNA polymerase. *J. Biol. Chem.*, **283**, 14411–14416.
2. Washington,M.T., Helquist,S.A., Kool,E.T., Prakash,L. and Prakash,S. (2003) Requirement of Watson-Crick hydrogen bonding for DNA synthesis by yeast DNA polymerase eta. *Mol. Cell. Biol.*, **23**, 5107–5112.
3. Pelletier,H., Sawaya,M.R., Kumar,A., Wilson,S.H. and Kraut,J. (1994) Structures of ternary complexes of rat DNA polymerase beta, a DNA template-primer, and ddCTP. *Science*, **264**, 1891–1903.
4. Bebenek,K., Beard,W.A., Darden,T.A., Li,L., Prasad,R., Luton,B.A., Gorenstein,D.G., Wilson,S.H. and Kunkel,T.A. (1997) A minor groove binding track in reverse transcriptase. *Nat. Struct. Biol.*, **4**, 194–197.
5. Kool,E.T. (2001) Hydrogen bonding, base stacking, and steric effects in dna replication. *Annu. Rev. Biophys. Biomol. Struct.*, **30**, 1–22.
6. Feng,J.Y. and Anderson,K.S. (1999) Mechanistic studies comparing the incorporation of (+) and (-) isomers of 3TCTP by HIV-1 reverse transcriptase. *Biochemistry*, **38**, 55–63.
7. Feng,J.Y., Shi,J., Schinazi,R.F. and Anderson,K.S. (1999) Mechanistic studies show that (-)-FTC-TP is a better inhibitor of HIV-1 reverse transcriptase than 3TC-TP. *FASEB J.*, **13**, 1511–1517.
8. Gumina,G., Chong,Y., Choo,H., Song,G.Y. and Chu,C.K. (2002) L-nucleosides: antiviral activity and molecular mechanism. *Curr. Top. Med. Chem.*, **2**, 1065–1086.
9. Chang,C.N., Skalski,V., Zhou,J.H. and Cheng,Y.C. (1992) Biochemical pharmacology of (+)- and (-)-2′,3′-dideoxy-3′-thiacytidine as anti-hepatitis B virus agents. *J. Biol. Chem.*, **267**, 22414–22420.
10. Schinazi,R.F., McMillan,A., Cannon,D., Mathis,R., Lloyd,R.M., Peck,A., Sommadossi,J.P., St Clair,M., Wilson,J., Furman,P.A. *et al.* (1992) Selective inhibition of human immunodeficiency viruses by racemates and enantiomers of cis-5-fluoro-1-[2-(hydroxymethyl)-1,3-oxathiolan-5-yl]cytosine. *Antimicrob. Agents Chemother.*, **36**, 2423–2431.
11. Joyce,C.M. and Benkovic,S.J. (2004) DNA polymerase fidelity: kinetics, structure, and checkpoints. *Biochemistry*, **43**, 14317–14324.
12. Moyle,G. (2000) Toxicity of antiretroviral nucleoside and nucleotide analogues: is mitochondrial toxicity the only mechanism? *Drug Saf.*, **23**, 467–481.
13. Olivero,O.A., Shearer,G.M., Chougnet,C.A., Kovacs,A.A., Landay,A.L., Baker,R., Stek,A.M., Khoury,M.M., Proia,L.A., Kessler,H.A. *et al.* (1999) Incorporation of zidovudine into leukocyte DNA from HIV-1-positive adults and pregnant women, and cord blood from infants exposed in utero. *AIDS*, **13**, 919–925.
14. Wutzler,P. and Thust,R. (2001) Genetic risks of antiviral nucleoside analogues–a survey. *Antiviral Res.*, **49**, 55–74.
15. Johnson,A.A., Ray,A.S., Hanes,J., Suo,Z., Colacino,J.M., Anderson,K.S. and Johnson,K.A. (2001) Toxicity of antiviral nucleoside analogs and the human mitochondrial DNA polymerase. *J. Biol. Chem.*, **276**, 40847–40857.
16. Feng,J.Y., Murakami,E., Zorca,S.M., Johnson,A.A., Johnson,K.A., Schinazi,R.F., Furman,P.A. and Anderson,K.S. (2004) Relationship between antiviral activity and host toxicity: comparison of the incorporation efficiencies of 2′,3′-dideoxy-5-fluoro-3′-thiacytidine-triphosphate analogs by human immunodeficiency virus type 1 reverse transcriptase and human mitochondrial DNA polymerase. *Antimicrob. Agents Chemother.*, **48**, 1300–1306.
17. Brown,J.A., Pack,L.R., Fowler,J.D. and Suo,Z. (2011) Pre-steady-state kinetic analysis of the incorporation of anti-HIV nucleotide analogs catalyzed by human X- and Y-family DNA polymerases. *Antimicrob. Agents Chemother.*, **55**, 276–283.
18. Brown,J.A., Pack,L.R., Fowler,J.D. and Suo,Z. (2012) Presteady state kinetic investigation of the incorporation of anti-hepatitis B nucleotide analogues catalyzed by noncanonical human DNA polymerases. *Chem. Res. Toxicol.*, **25**, 225–233.
19. Vyas,R., Zahurancik,W.J. and Suo,Z. (2014) Structural basis for the binding and incorporation of nucleotide analogs with L-stereochemistry by human DNA polymerase lambda. *Proc. Natl. Acad. Sci. U.S.A.*, **111**, E3033–E3042.
20. Gaur,V., Vyas,R., Fowler,J.D., Efthimiopoulos,G., Feng,J.Y. and Suo,Z. (2014) Structural and kinetic insights into binding and incorporation of L-nucleotide analogs by a Y-family DNA polymerase. *Nucleic Acids Res.*, **42**, 9984–9995.
21. Vyas,R., Reed,A.J., Tokarsky,E.J. and Suo,Z. (2015) Viewing human DNA polymerase beta faithfully and unfaithfully bypass an oxidative lesion by time-dependent crystallography. *J. Am. Chem. Soc.*, **137**, 5225–5230.
22. Freudenthal,B.D., Beard,W.A., Shock,D.D. and Wilson,S.H. (2013) Observing a DNA polymerase choose right from wrong. *Cell*, **154**, 157–168.
23. Pelletier,H., Sawaya,M.R., Wolfle,W., Wilson,S.H. and Kraut,J. (1996) Crystal structures of human DNA polymerase beta complexed with DNA: implications for catalytic mechanism, processivity, and fidelity. *Biochemistry*, **35**, 12742–12761.
24. Batra,V.K., Beard,W.A., Shock,D.D., Krahn,J.M., Pedersen,L.C. and Wilson,S.H. (2006) Magnesium-induced assembly of a complete DNA polymerase catalytic complex. *Structure*, **14**, 757–766.
25. Sawaya,M.R., Prasad,R., Wilson,S.H., Kraut,J. and Pelletier,H. (1997) Crystal structures of human DNA polymerase beta complexed with gapped and nicked DNA: evidence for an induced fit mechanism. *Biochemistry*, **36**, 11205–11215.
26. Battye,T.G., Kontogiannis,L., Johnson,O., Powell,H.R. and Leslie,A.G. (2011) iMOSFLM: a new graphical interface for

diffraction-image processing with MOSFLM. *Acta Crystallogr. D Biol. Crystallogr.*, **67**, 271–281.
27. McCoy,A.J., Grosse-Kunstleve,R.W., Adams,P.D., Winn,M.D., Storoni,L.C. and Read,R.J. (2007) Phaser crystallographic software. *J. Appl. Crystallogr.*, **40**, 658–674.
28. Murshudov,G.N., Skubak,P., Lebedev,A.A., Pannu,N.S., Steiner,R.A., Nicholls,R.A., Winn,M.D., Long,F. and Vagin,A.A. (2011) REFMAC5 for the refinement of macromolecular crystal structures. *Acta Crystallogr. D Biol. Crystallogr.*, **67**, 355–367.
29. Emsley,P. and Cowtan,K. (2004) Coot: model-building tools for molecular graphics. *Acta Crystallogr. D Biol. Crystallogr.*, **60**, 2126–2132.
30. Laskowski,R.A., Rullmannn,J.A., MacArthur,M.W., Kaptein,R. and Thornton,J.M. (1996) AQUA and PROCHECK-NMR: programs for checking the quality of protein structures solved by NMR. *J. Biomol. NMR*, **8**, 477–486.
31. DeLano,W.L. (2002) DeLano Scientific, San Carlos.
32. Sohl,C.D., Szymanski,M.R., Mislak,A.C., Shumate,C.K., Amiralaei,S., Schinazi,R.F., Anderson,K.S. and Yin,Y.W. (2015) Probing the structural and molecular basis of nucleotide selectivity by human mitochondrial DNA polymerase gamma. *Proc. Natl. Acad. Sci. U.S.A.*, **112**, 8596–8601.
33. DeLucia,A.M., Chaudhuri,S., Potapova,O., Grindley,N.D. and Joyce,C.M. (2006) The properties of steric gate mutants reveal different constraints within the active sites of Y-family and A-family DNA polymerases. *J. Biol. Chem.*, **281**, 27286–27291.
34. Wang,W., Wu,E.Y., Hellinga,H.W. and Beese,L.S. (2012) Structural factors that determine selectivity of a high fidelity DNA polymerase for deoxy-, dideoxy-, and ribonucleotides. *J. Biol. Chem.*, **287**, 28215–28226.
35. Brown,J.A., Duym,W.W., Fowler,J.D. and Suo,Z. (2007) Single-turnover kinetic analysis of the mutagenic potential of 8-oxo-7,8-dihydro-2′-deoxyguanosine during gap-filling synthesis catalyzed by human DNA polymerases lambda and beta. *J. Mol. Biol.*, **367**, 1258–1269.
36. Garcia-Diaz,M., Bebenek,K., Krahn,J.M., Kunkel,T.A. and Pedersen,L.C. (2005) A closed conformation for the Pol lambda catalytic cycle. *Nat. Struct. Mol. Biol.*, **12**, 97–98.
37. Beard,W.A. and Wilson,S.H. (2014) Structure and mechanism of DNA polymerase beta. *Biochemistry*, **53**, 2768–2780.
38. Tsai,Y.C. and Johnson,K.A. (2006) A new paradigm for DNA polymerase specificity. *Biochemistry*, **45**, 9675–9687.
39. Showalter,A.K. and Tsai,M.D. (2002) A reexamination of the nucleotide incorporation fidelity of DNA polymerases. *Biochemistry*, **41**, 10571–10576.
40. Wong,I., Patel,S.S. and Johnson,K.A. (1991) An induced-fit kinetic mechanism for DNA replication fidelity: direct measurement by single-turnover kinetics. *Biochemistry*, **30**, 526–537.
41. Johnson,K.A. (1993) Conformational coupling in DNA polymerase fidelity. *Annu. Rev. Biochem.*, **62**, 685–713.
42. Xiang,Y., Goodman,M.F., Beard,W.A., Wilson,S.H. and Warshel,A. (2008) Exploring the role of large conformational changes in the fidelity of DNA polymerase beta. *Proteins*, **70**, 231–247.
43. Moscato,B., Swain,M. and Loria,J.P. (2016) Induced fit in the selection of correct versus incorrect nucleotides by DNA polymerase beta. *Biochemistry*, **55**, 382–395.
44. Evans,G.W., Hohlbein,J., Craggs,T., Aigrain,L. and Kapanidis,A.N. (2015) Real-time single-molecule studies of the motions of DNA polymerase fingers illuminate DNA synthesis mechanisms. *Nucleic Acids Res.*, **43**, 5998–6008.
45. Luo,G., Wang,M., Konigsberg,W.H. and Xie,X.S. (2007) Single-molecule and ensemble fluorescence assays for a functionally important conformational change in T7 DNA polymerase. *Proc. Natl. Acad. Sci. U.S.A.*, **104**, 12610–12615.
46. Krahn,J.M., Beard,W.A. and Wilson,S.H. (2004) Structural insights into DNA polymerase beta deterrents for misincorporation support an induced-fit mechanism for fidelity. *Structure*, **12**, 1823–1832.
47. Beard,W.A., Shock,D.D., Batra,V.K., Prasad,R. and Wilson,S.H. (2014) Substrate-induced DNA polymerase beta activation. *J. Biol. Chem.*, **289**, 31411–31422.
48. Washington,M.T., Prakash,L. and Prakash,S. (2001) Yeast DNA polymerase eta utilizes an induced-fit mechanism of nucleotide incorporation. *Cell*, **107**, 917–927.
49. Xu,C., Maxwell,B.A. and Suo,Z. (2014) Conformational dynamics of Thermus aquaticus DNA polymerase I during catalysis. *J. Mol. Biol.*, **426**, 2901–2917.